

A DUAL-SCALE THREE-PHASE FLOW-STRESS MODEL FOR PREPREG PROCESSING

Shayan Fahimi^{1*}, Anoush Poursartip¹, Reza Vaziri¹

¹ Composites Research Network, The University of British Columbia, Vancouver, BC, V6T 1Z4, Canada

* Corresponding author (shayan@composites.ubc.ca)

Keywords: *prepreg processing, dual-scale, integrated flow-stress model*

ABSTRACT

The outcome of a manufactured composite part is, to a large extent, determined by the phenomena that take place during the early stages of processing when the resin is in a pre-gelled state and gas can escape from the intra-tow regions and channels to the vents. This work introduces a dual-scale representation of porosity implemented in the 3-phase integrated flow-stress model (3PIFS) for simulating the capillary effect and intra-tow gas transport in composite processing. One-dimensional elements, formulated based on earlier work in the LCM literature, are used to represent the resin flow inside tows while the resin flow in channels and porous media consolidation in the global domain are represented by the original integrated flow-stress (IFS) model. The results of the current dual-scale model are compared with the original IFS model to highlight the effect of microscale resin flow and gas depletion during the pre-gelation phase.

1 INTRODUCTION

In prepreg processing, vacuum pressure is the driving force for reducing porosity through the removal of gas and dissolved volatiles. On the other hand, local changes in resin pressure due to macroscale and microscale geometric features can cause void formation and growth [1], [2]. Porosity can significantly deteriorate the mechanical performance of composite parts and predicting resin pressure and gas distribution can help manufacturers to minimize the probability of excessive porosity. Therefore, many studies have focused on predicting the resin and capillary pressure effects on porosity during processing, e.g., [3], [4].

During the debulking stage, most of the air, entrapped between the plies during deposition, is removed and the part thickness is reduced. However, bubbles in local channels may not find a continuous path to the vacuum system and remain entrapped in the composite part. During the early stages of a cure cycle, as the resin viscosity decreases, the resin flows more easily within the global channels, which are incorporated in the prepreg to facilitate air removal. Higher temperatures increase the vapor pressure of the volatiles in the resin and result in the diffusion of volatiles in the existing gas bubbles. Bubbles that are far from vacuum ports need more time to join the newly created channels, thus, the processing window should give them enough time to convect through the channels and reach evacuation ports. By the end of the processing window, when most of the resin is cured and crosslinked, the remaining bubbles cannot move toward the vacuum ports anymore and manifest as the final porosity of the composite part.

Previous studies show that the capillary effect induces pressures comparable to the total pressure or Darcy's pressure at the intra-tow level [4]. By invoking either a hydrodynamic or hydrostatic assumption, Zobeiry and Duffner [4] showed, that the thermodynamic pressure has a negative correlation with the radius of curvature at the contact angle of two fibers and found the pressure to be around -250 kPa at a radius of curvature of 180 nm. The effect of capillary pressure is not as significant at the inter-tow level and can be neglected. To incorporate the effects of capillary pressure on resin percolation and gas entrapment, we need to represent intertow (global) and intratow (local) regions separately in the numerical model.

To clarify the difference between channels and intratow regions, Figure 1 shows schematically the state of gas bubbles and channels while a layer of prepreg is being compressed by applied pressure on

the top surface. In Stage (a), just before the application of pressure, gas bubbles are present in channels and intratow regions and channels are fully open. Shortly after applying the pressure, Stage (b), most of the gas in the global channels is depleted and the channels begin to collapse. If all the gas remains in pressure equilibrium with resin, as would be the case when all the gas exists in the global channels, gas will quickly deplete due to its lower viscosity and the compaction of channels occurs instantaneously (as is the case in the original 3PIFS). However, if we keep some gas in the local scale and assign a low value of permeability to the constituents at this scale, gas bubbles will slowly move towards the channels and the compaction continues for a period of time (Stage c). If resin does not solidify, all bubbles will eventually find their way to the vent and leave the system. However, in a cure cycle, bubbles have a limited time to flow to the boundaries and will be entrapped within the global or local scale after solidification (Stage d).

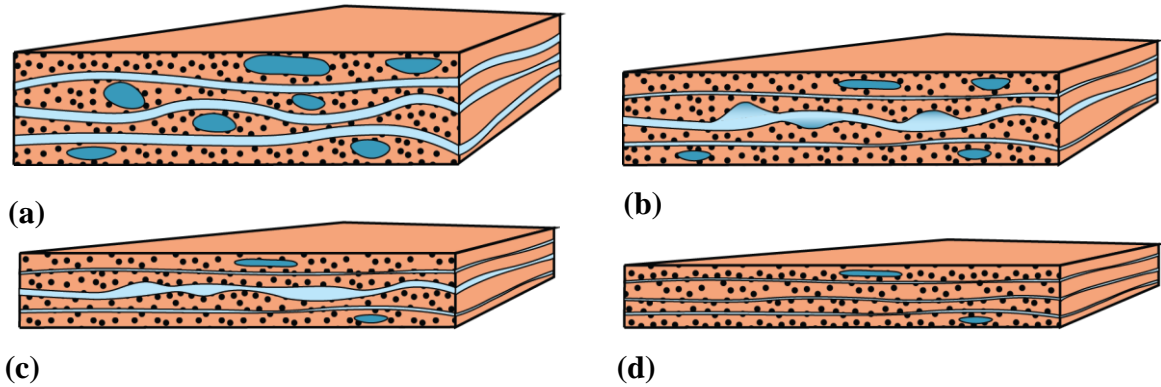


Figure 1: Schematic showing four stages of compaction due to external load on the top surface during the cure cycle; Stage (a): gas bubbles are present in both scales before debulk, Stage (b): gas in the global channels are depleted shortly after applying pressure, Stage (c): gas in the local, intra-tow, domain move to channels and out of the system at the pre-gelation phase, Stage (d): gas bubbles are entrapped when resin solidifies

In the next section, we will present the mathematical formulation of the local 1D element, adopted from the liquid composite molding (LCM) literature, which has been incorporated into the current macroscopic process modelling framework to enable the flow of gas relative to the resin. The air entrapment parameter that appears in such formulation was assumed to be a constant value in the LCM literature. A method for updating the air entrapment parameter based on the solidification and saturation of resin at the local scale is presented in the second part of this section. Two numerical examples are presented in Section 3 to demonstrate the role of microscale elements during the curing and consolidation of prepreg.

2 PROBLEM FORMULATION

The latest formulation of the IFS model couples Darcy's law with the conservation of mass and momentum (equilibrium of forces) [5]. The transition of liquid resin to solid resin is incorporated in the IFS model by introducing a new scalar quantity, λ , termed 'solidification factor', which is bounded between zero and one ($\lambda = 0$ for unsolidified resin and $\lambda = 1$ for fully solidified resin) [6], [7]. As saturation of fiber tows takes place at a much slower rate than the channels, we modified the existing formulation by adding 1D elements to each node, which represents the intra-tow capillary effect at the microscale and captures local gas flow and entrapment.

The capillary pressure is represented as an extra force on 1D elements that either pulls the resin inside fiber tows or prevents the resin from entering the tows. Using the air entrapment parameter, δ , any impregnation scenario of the intra-tow region is a weighted average of the two bounds. The air entrapment parameter depends on the resin state variables, e.g. resin saturation, tracked at the macroscale element nodes. When the saturation, ψ^r , exceeds a certain threshold, ψ^* , resin entraps gas bubbles and gas cannot infiltrate into the channels and escape into the global domain.

As shown in Eqs. 1 and 2, as resin infiltrates the tows, the intra-tow pressure, P^{tow} , increases to a level that eventually approaches the global resin pressure, P^r .

$$P^{tow} = (1 - \delta)P_{lower}^{tow} + \delta P_{upper}^{tow} \quad (1)$$

$$P_{lower}^{tow} = P^{in} - P^c, P_{upper}^{tow} = \min \left| \frac{P^v}{1 - \psi^{tow}} - P^c, P^r \right| \quad (2)$$

The lower limit of tow pressure, P_{lower}^{tow} , is equal to the vent pressure, P^v , unless the capillary pressure, P^c , is also accounted for in the microscale. While the lower tow pressure does not depend on the saturation at the microscale, the upper tow pressure is primarily a function of the vent pressure and the saturation in microscale or intra-tow saturation, ψ^{tow} . Since the pressure at the interface of resin and gas in the microscale cannot exceed the surrounding fluid pressure or the global pressure P^r , the upper tow pressure is bounded by the global resin pressure. The air entrapment parameter, δ , is used to control the tow pressure based on the ability of air to escape the intra-tow region. When $\delta = 1$, resin entraps gas bubbles and gas cannot infiltrate into the channels and escape into the global domain. Darcy's law is solved over the incorporated 1D elements to find the flow of resin into the tows caused by the difference between the global resin pressure, P^r , and the local pressure, P^{tow} . A trigger node at the end of the local elements prevents further flow of resin into the tows when they are saturated [8].

2.1 Air entrapment parameter

While the air entrapment parameter is assumed to be constant in the LCM literature [8], the experimental evidence in the literature [9], [10] suggests that the air entrapment parameter should be directly proportional to the saturation of resin and the solidification factor. A logistic regression function (Eq. 3) describes a nonlinear relationship between the air entrapment parameter and solidification or saturation, where the rate of change of air entrapment is maximum right at the middle of the pre-gelation phase:

$$\delta = \delta_\psi \delta_\lambda \quad (3)$$

$$\delta_\psi = \frac{1}{1 + e^{-k_1(\psi - \psi_0)}}, \delta_\lambda = \frac{1}{1 + e^{-k_2(\lambda - \lambda_0)}} \quad (4)$$

In the above equations, δ_ψ and δ_λ are air entrapment parameters due to the saturation and solidification factor at a node, ψ_0 is the saturation when $\delta_\psi = 0.5$ and is assumed to be an approximated average of the resin saturation at the start and end of the cure cycle, $\lambda_0 = 0.5$, and k_1 and k_2 are rates of growth of the logistic regression function that should be characterized for the composite system. In Fig. 2, the contour of the air entrapment parameter is shown as a function of saturation and solidification for a possible set of air entrapment parameters: $\lambda_0 = 0.5$, $\psi_0 = 0.9$, $k_1 = 60$, and $k_2 = 12$.

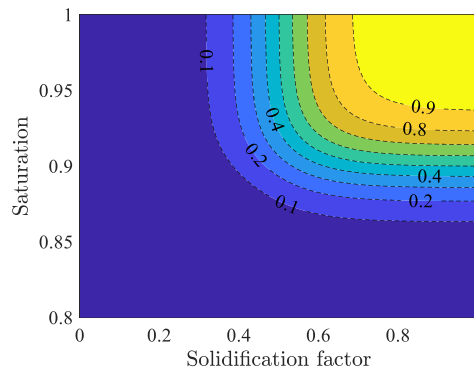


Figure 2: Air entrapment parameter (δ) as a function of saturation and solidification factor for the case where $\lambda_0 = 0.5$, $\psi_0 = 0.9$, $k_1 = 60$, and $k_2 = 12$

With these set of parameters, the air entrapment parameter is zero in a bigger portion of the feasible region (dark blue region). When δ is small in a bigger portion of this region, the difference between the tow and channel pressures is higher and the gas in the local elements escapes faster to the global channels. To better demonstrate the effects of 1D local elements with changing air entrapment parameters, two numerical tests are conducted, which will be described in the next section.

3 NUMERICAL EXAMPLES

The numerical examples demonstrate the role of microscale elements during the curing process and the response of the 3PIFS model for a composite column undergoing consolidation and cure. The composite material is AS4/3501-6 prepreg [11] with various degrees of saturation. The air properties are obtained from Dixon [12] and shown in Table 1, where the temperatures are in °C. The permeability of each phase at a node in the microscale is assumed to be six order of magnitude smaller than (i.e. a factor of 10^{-6} times) the permeability of the phase calculated for the global domain [9]. In the first example, the pressure and displacement of a column of prepreg during the debulking process obtained by the original and multiscale 3PIFS are compared. The same column goes through a one-hold cure cycle in the second example.

Table 1: Properties of air [12]

Properties	Value
Bulk modulus (GPa)	The absolute pressure of air
Shear modulus (GPa)	1×10^{-11}
Volumetric coefficient of thermal expansion (/°C)	$\alpha_{th}^a = \frac{1}{T}$
Air viscosity (Pa.s)	$\mu = \frac{1.458 \times 10^{-6} T^{1.5}}{110.4 + T}$

3.1. Debulking of a column of partially saturated prepreg

In this example, the debulking process of a column of partially saturated and unsolidified prepreg under uniform pressure is simulated. The top surface is subjected to a loading of 50 kPa and is permeable. The simulation is performed at a constant temperature of 20°C and the column is discretized using 20 elements in the vertical direction and 3 elements in the horizontal direction (Figure 3). The viscosities of resin and air are $1.177 \times 10^4 Pa.s$ and 1.813×10^{-5} at 20°C and do not change during the analysis. The initial fiber volume fraction is 0.58, which means that the total volume fraction of both fluids, resin and air, is 0.42 ($\varphi_0^r + \varphi_0^g = 0.42$). The analysis is performed in ABAQUS with a fixed timestep of $\Delta t = 1 \times 10^{-7} s$ to capture the initial compaction of the laminate. Based on the values reported in [4], the capillary ratio is assumed to be 0.1, meaning that the capillary pressure is 10 times lower than the pressure in the macroscale at any node. In all cases studied here, when the gas content is not zero, the current model initializes with a gas content of 25% in local elements.

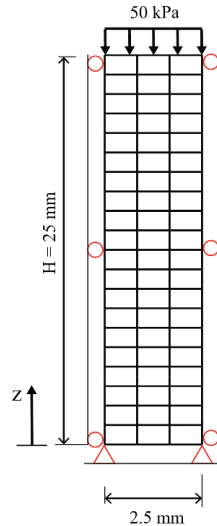


Figure 3: Geometry and boundary conditions of an unsolidified and partially saturated column representing a column of prepreg

Figure 4 shows the predicted pressure at different heights in the prepreg column for three different values of initial air content (φ_0^g) just after the load is applied. The prepreg column, which is effectively a compressible Terzaghi's column [13], shows an instantaneous pressure drop that is directly proportional to the air content of the system. The pressure at the top permeable surface, $\frac{z}{H} = 1$, is zero to satisfy the boundary condition. The lower pressure predicted at higher air contents reflects the effect of the compressibility of the gas phase which results in sharing a greater portion of pressure with the fiber-bed.

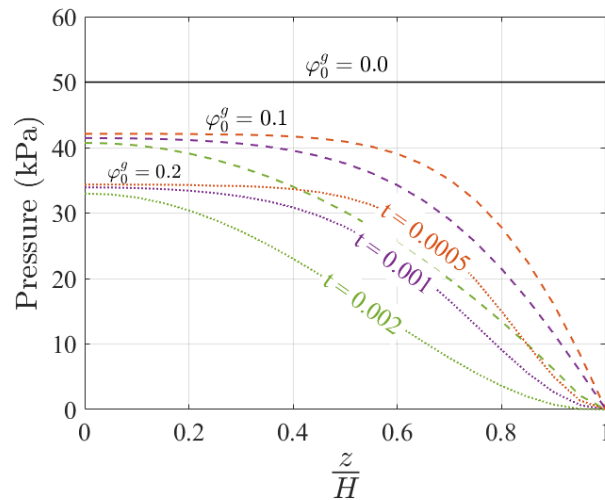


Figure 4: The predicted global pressure at different heights in the column of the partially saturated prepreg for different initial air volume fractions (φ_0^g)

The pressure predicted in the current work is compared with the original 3PIFS [3] in Figure 5. It is evident that the pressure drop in the current model is less severe, as the compaction of 1D elements is taking place at different timescales, occurring much more slowly than the compaction of channels at the global scale.

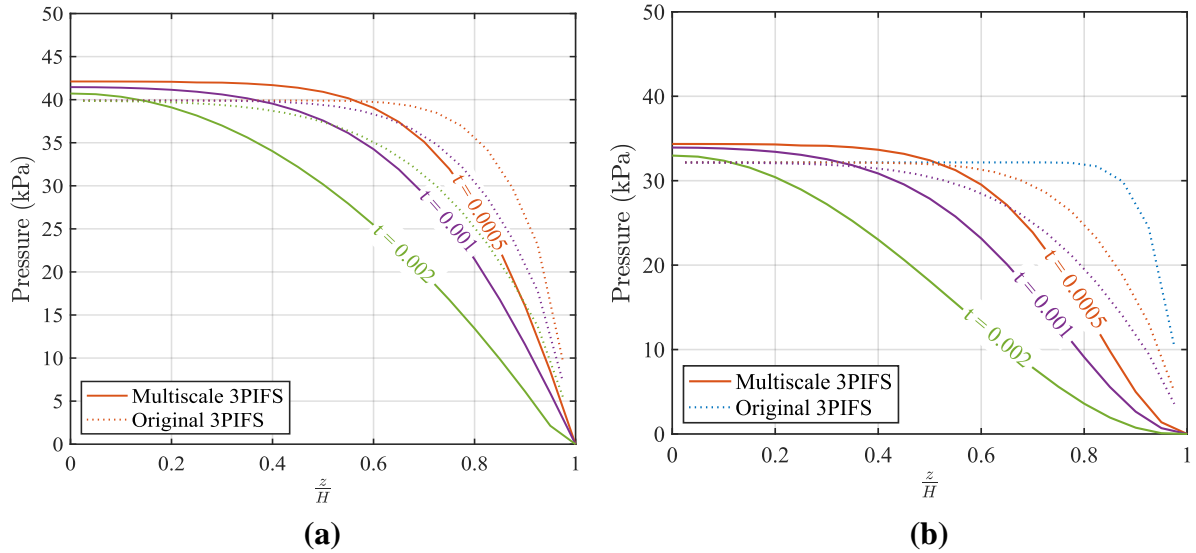


Figure 5: Comparison of the predicted pressure versus height at (a) 10% gas content, ($\varphi_0^g = 0.1$) and (b) 20% gas content, ($\varphi_0^g = 0.2$) obtained from the current multiscale 3PIFS and the original 3PIFS [6]

The displacement at the top surface versus time is shown in Figure 6. The higher compressibility of the gas phase comes into play as the column is consolidated more severely within the same time frame. The figure also shows the results of the original flow-stress model. In the current model (multiscale 3PIFS), the displacement exhibits a more gradual change due to the relaxation-like behavior caused by the varying consolidation timescales of the 1D elements. The increased consolidation rate predicted by the current model in the asymptotic part of the graph (further to the right of the time axis) is primarily attributed to escape of gas from the local elements. This is because the permeability of air is mainly due to the gas escaping from the local elements since the permeability of air is greater than resin by a few orders of magnitude.

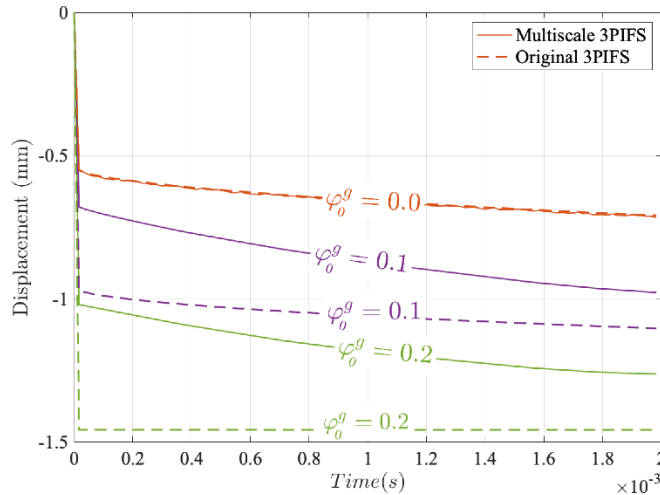


Figure 6: The predicted displacement of the top surface of the column of partially saturated prepreg at the beginning of consolidation for different initial air volume fractions (φ_0^g)

In Figure 6, the sudden drop in displacement at the start of the analysis is indicative of gas escape from the global channels, demonstrated as Stage (b) in Figure 1. The gradual decrease in the magnitude of displacement in the rest of the graph can be attributed to the migration of gas from the microscale to the macroscale, demonstrated as Stage (c) in Figure 1. Since the original 3PIFS has no means of accounting for this form of gas transportation, it overestimates the drop in displacement at the beginning of the analysis and is not able to capture the ensuing gradual change in consolidation.

3.2. Curing of a column of partially saturated resin

In this section, the model shown in Figure 3 goes through a one-hold cure cycle, as shown in Figure 7, while the loading on the top surface is removed, to investigate the effects of the new solidification factor and 1D gas elements on the response of the column during the curing process. It is important to note that no inertia effect is included in the momentum conservation (equilibrium equation) of the 3PIFS model.

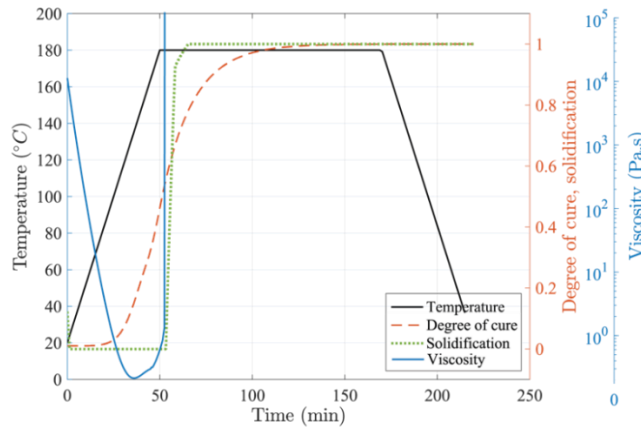


Figure 7: The time history of temperature, DOC, solidification, and viscosity in the one-hold cure cycle applied to a column of partially saturated resin

Figure 8 compares the transverse strains computed using the current model with the one computed with the original 3PIFS. The system either contains only resin ($\varphi_0^r = 0.42$) or 10% gas ($\varphi_0^r = 0.32, \varphi_0^g = 0.1$) and the top surface is impermeable. With an impermeable boundary condition, the thermal expansion during the heat-up regime induces significant amounts of transverse strain. With some air in the system, the system expands even further since the thermal expansion coefficient of air is higher than resin. When the DOC of the sample increases, the cure shrinkage effect reduces the transverse strain. The effect of cure shrinkage is lower when some amount of air is in the system. Since the thermal properties of the fiber, resin, and gas used in this work are identical to the ones used in the original 3PIFS model, the results of the two models coincide when no gas is present in the system. The local elements are also under nonzero capillary pressure (assumed to be 10 kPa); thus, resin still infiltrates the tows. The transverse strain at the beginning of the cure cycle, where resin is infiltrating the intra-tow regions, is lower in the current multiscale model.

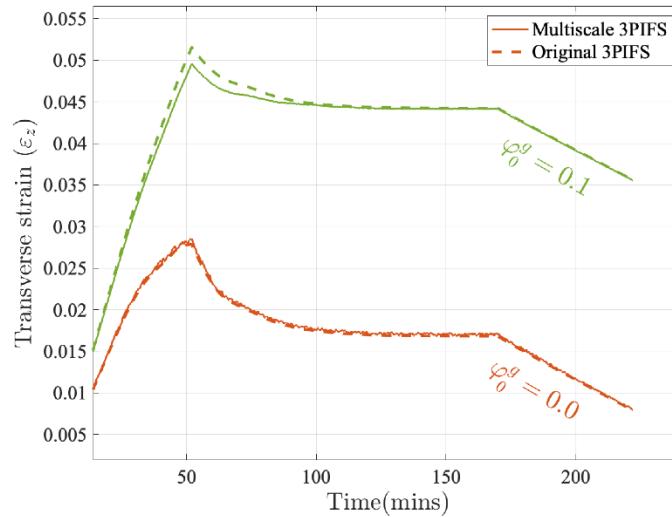


Figure 8: The transverse strain at the top of the partially saturated column (impermeable top surface)

With a permeable top surface (Figure 9), the fully saturated sample shows considerable tensile strain due to the higher viscosity of resin at the beginning of the analysis. The transverse strain obtained in the current work is different from the results of the original 3PIFS, particularly during the heat-up portion of the cure cycle. The difference is due to the slightly different method of finding the effective material properties of the prepreg, described in the previous chapter, and the viscoelastic constitutive material model used in this work.

When some air is added to the system, the amount of air entrapped in the local elements is the main cause of the difference between the current and the original 3PIFS model. In the original model, air could promptly evacuate the system via the top permeable surface, since air and resin pressures were considered to be equal and the viscosity of air is very low. Thus, with air in the system, the transverse strain at the start of the curing process was significantly lower than the fully saturated sample.

In the current model, the lower permeability of the local elements and higher air entrapment values delays the evacuation of air entrapped from the local channels to the global channels. Higher air content increases the transverse strain due to the thermal expansion of the entrapped air and reduces the role of cure shrinkage, as shown in Figure 9. In this figure, “global gas escape only” shows the results when gas bubbles in the local elements are disconnected from the global channels (by assuming $\delta = 1$), and therefore cannot leave the system.

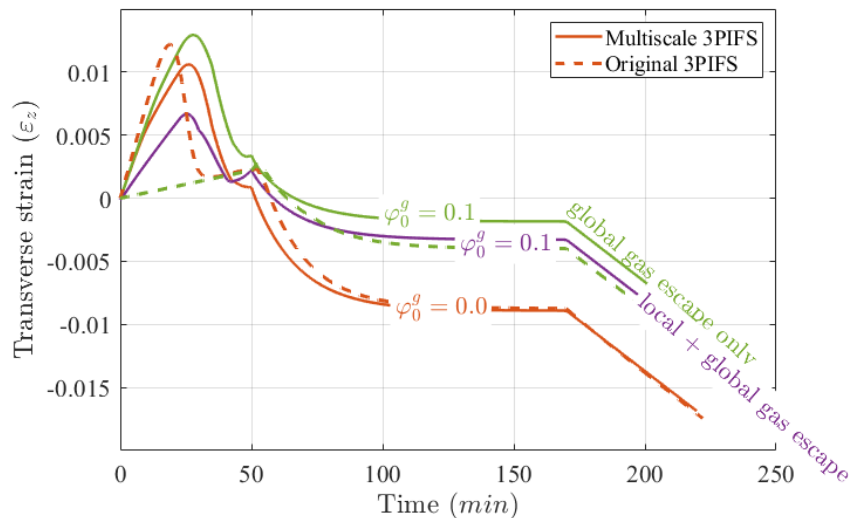


Figure 9: The transverse strain at the top surface of the partially saturated column (permeable top surface)

4 CONCLUSIONS

Local changes in resin pressure can cause void formation and growth, leading to excessive porosity and deterioration in the mechanical performance of the composite part. Predicting local resin pressure and gas distribution can help us to minimize the probability of excessive porosity. This work enhances the current state-of-the-art in the 3-phase integrated flow-stress (3PIFS) modelling by adding one-dimensional elements to represent the effect of resin flow in the intra-tow regions (microscale) on the transverse strain and pressure at the global scale. At the macroscale, gas and resin are described with a single Darcy's equation (3PIFS formulation), and at the microscale, one-dimensional local elements are added to the global elements to represent the flow of gas and resin stored in the intra-tow region.

With this multiscale model, the effect of slower tow-saturation and gas evacuation at the intra-tow scale is better represented in the 3PIFS model. When the current model is used to simulate the debulking of a column of partially saturated prepreg, it is shown that this model predicts a less severe pressure drop and a more gradual consolidation compared to the original flow-stress model (3PIFS). The compaction of 1D elements occurs much more slowly than the compaction of channels at the macroscale. The consolidation observed after the sudden drop in displacement at the beginning of the analysis, representing air migration from the macroscale, indicates the stage where gas in the microscale moves to the channels and eventually out of the system in the pre-gelation phase. Moreover, the transverse strain of partially saturated resin under no loading during a one-hold cure cycle is studied with different gas contents and permeable/impermeable top surfaces. The results showed a higher change in the transverse strain than that predicted by the original 3PIFS model during the heat-up ramp due to the thermal expansion of entrapped air in the local scale.

REFERENCES

- [1] H. Bedayat *et al.*, "Simulation of Gas and Resin Transport Mechanisms in Manufacturing Process of Composite Structures and Their Effect on Porosity," *Proceedings of the American Society for Composites — Thirty-second Technical Conference*, vol. 0, no. 0, 2017, Accessed: Jan. 09, 2018. [Online]. Available: <http://dpi-proceedings.com/index.php/asc32/article/view/15212>
- [2] M. Roy, "Porosity in configured structures : effect of ply drops and caul sheets in the processing of composite parts," Ph.D. Thesis, University of British Columbia, 2015. Accessed: Oct. 24, 2017. [Online]. Available: <https://open.library.ubc.ca/cIRcle/collections/ubctheses/24/items/1.0220869>

- [3] S. A. Niaki, A. Forghani, R. Vaziri, and A. Poursartip, "A three-phase integrated flow-stress model for processing of composites," *Mechanics of Materials*, vol. 117, pp. 152–164, Feb. 2018,
- [4] N. Zobeiry and C. Duffner, "Measuring the negative pressure during processing of advanced composites," *Composite Structures*, vol. 203, pp. 11–17, Nov. 2018,
- [5] S. Amini Niaki, A. Forghani, R. Vaziri, and A. Poursartip, "An Orthotropic Integrated Flow-Stress Model for Process Simulation of Composite Materials—Part II: Three-Phase Systems," *Journal of Manufacturing Science and Engineering*, vol. 141, no. 3, Jan. 2019, Accessed: Apr. 20, 2022. [Online]. Available: <https://doi.org/10.1115/1.4041862>
- [6] S. Amini Niaki, "A three-phase integrated flow-stress framework for process modelling of composite materials," Ph.D. Thesis, University of British Columbia, 2017. Accessed: Oct. 24, 2017. [Online]. Available: <https://open.library.ubc.ca/cIRcle/collections/ubctheses/24/items/1.0355735>
- [7] S. A. Niaki, A. Forghani, R. Vaziri, and A. Poursartip, "A two-phase integrated flow-stress process model for composites with application to highly compressible phases," *Mechanics of Materials*, vol. 109, pp. 51–66, Jun. 2017,
- [8] J. M. Lawrence, V. Neacsu, and S. G. Advani, "Modeling the impact of capillary pressure and air entrapment on fiber tow saturation during resin infusion in LCM," *Composites Part A: Applied Science and Manufacturing*, vol. 40, no. 8, pp. 1053–1064, Aug. 2009,
- [9] H. Tan and K. M. Pillai, "Multiscale modeling of unsaturated flow in dual-scale fiber preforms of liquid composite molding I: Isothermal flows," *Composites Part A: Applied Science and Manufacturing*, vol. 43, no. 1, pp. 1–13, Jan. 2012,
- [10] M. Mohseni, N. Zobeiry, and G. Fernlund, "Experimental and numerical study of coupled gas and resin transport and its effect on porosity," *Journal of Reinforced Plastics and Composites*, vol. 38, no. 23–24, pp. 1055–1066, Dec. 2019,
- [11] "RAVEN v3.12.3." Convergent Manufacturing Technologies, 2020. Accessed: Jan. 17, 2020. [Online]. Available: <https://www.convergent.ca/products/raven-simulation-software>
- [12] J. C. Dixon, *The Shock Absorber Handbook*. Chichester, UK: John Wiley & Sons, Ltd, 2007. Accessed: Nov. 27, 2018. [Online]. Available: <http://doi.wiley.com/10.1002/9780470516430>
- [13] S. M. Haghshenas, R. Vaziri, and A. Poursartip, "Integration of resin flow and stress development in process modelling of composites: Part II – Transversely isotropic formulation," *Journal of Composite Materials*, p. 0021998318762296, Mar. 2018,